ELSEVIER

Chemical Engineering Journal 71 (1998) 175–182

Chemical Engineering Journal

Numerical computation of natural convection for a low-Prandtl-number fluid in a shallow rectangular region heated from below

Akihiro Nakano[a,*], Hiroyuki Ozoe[a], S.W. Churchill[b]

[a]*Institute of Advanced Material Study, Kyushu University, Kasuga Koen 6-1, Kasuga, 816, Japan*
[b]*Department of Chemical Engineering, University of Pennsylvania, Philadelphia, PA 19104, USA*

Received 1 July 1998; received in revised form 5 October 1998; accepted 14 October 1998

Abstract

Transient natural convection in a low-Prandtl-number fluid was computed for a shallow rectangular enclosure of $5 \times 5 \times 1$ heated from below and cooled from above with four dragless, adiabatic, vertical walls. The model consists of three-directional mass, momentum and energy balances. These equations were approximated by a HSMAC finite-difference method with a hybrid scheme for the inertial terms. Computations for $Ra = 2000$ and $Pr = 0.01$ required an accumulative time of two months. The transient response after a step increase of the lower-wall temperature was at first a regular oscillation, which then evolved to a series of long rolls with their axes in one direction. These transient characteristics of the velocity and temperature fields are presented graphically.

Keywords: Natural convection; Low-Prandtl-number

1. Introduction

The forced convective behavior of low-Prandtl-number fluids such as liquid metals and plasmas is known to differ functionally from that of high-Prandtl-number fluids. This difference in behavior might also be expected for natural convection. Liquid metals and molten semi-conducting materials have become key industrial materials, and their characteristics of heat and momentum transfer are important considerations in the design of manufacturing processes for more efficient operations and for products of higher quality. Examples are continuous steel-casting, float-casting of metals in a cold crucible and Czochralski crystal-growing. In these practical systems, inertial natural convection is dominant because the Prandtl number is of the order of 0.01. Natural convection in low-Prandtl-number fluids has been observed to be oscillatory [1,2] but the oscillatory characteristics themselves have not been clarified in detail. It is quite important to clarify these characteristics in order to obtain finely controlled high quality products such as a single-crystal rod of silicon for future ultra-large scale integrated electronic circuits.

There has been an extensive amount of work in the field of material science on the bulk growth of silicon single-crystal rods. However, there are many ambiguities and inconsistencies in even the recent reports [3–11], probably because of complicated manufacturing systems such as a Czochralski crystal-growing with buoyancy, separate rotations of the crystal rod, and radiative heating and cooling. The Lorentz force from a magnetic field makes the behavior even more complicated. The present authors have carried out numerical analyses of Czochralski crystal growing with and without magnetic fields [12–19]. That work suggests that a good understanding of oscillatory convection in liquid metals requires separate study in a more simplified geometrical system with a single body force. For such a reason we have turned back to the classical Rayleigh–Benard problem for a low-Prandtl-number fluid as described in the present paper.

Rayleigh–Benard natural convection in a shallow layer of fluid heated from below and cooled from above has been studied extensively but not in terms of the oscillatory characteristics of low-Prandtl-number fluids. The oscillatory convection of molten semi-conducting materials has been known and considered to be responsible for the undesirable striae in crystal rods [1]. Fundamental studies on oscillatory convection are expected to clarify the general mechanism of oscillatory convection and suggest effective ways for its control. Rayleigh–Benard natural convection was graphically classified by Krishnamurti [20] and the characteristics of low-Prandtl-number fluid have been studied extensively

*Corresponding author. Tel.: +81-92-583-7834; fax: +81-92-583-7838; e-mail: ozoe@cm.kyushu-u.ac.jp

1385-8947/98/$ – see front matter
PII: S1385-8947(98)00136-3

in a series of papers by Clever and Busse [21–23]. Some of the recent work on applications for material processing has been described by Müller et. al. [24] and a review has been presented by Ristorcelli and Lumley [25]. However, there are very few works on the experimental measurements of Rayleigh convection for low-Prandtl-number fluids except that by Rossby [26]. He studied Rayleigh–Benard natural convection experimentally in low-Prandtl-number fluids in a shallow layer with and without rotation. According to his results, irregular temperature fluctuations are to be expected even at only slightly supercritical Rayleigh numbers. Oscillatory natural convection of the low Prandtl number fluids heated from a vertical side wall [27–29] or from below [30] has also been studied by the present authors. For example, Okada and Ozoe [28] studied the effect of the computational scheme (central difference or hybrid scheme), four different grid sizes for the same system, three different time increments and three different initial conditions for oscillatory multiple roll cells in a rectangular shallow enclosure for a hypothetical fluid with a Prandtl number equal to zero. The most striking finding was that oscillatory convection may result from an increase in the grid numbers, i.e., no oscillation was computed at $Gr = 3 \times 10^4$ and an aspect ratio of three for the grid numbers of 61×21 and 75×25 in the horizontal and vertical directions, but standing oscillations were computed for grids of 105×35 and 121×41. At $Gr = 4 \times 10^4$, the amplitude of the maximum stream function increased almost ten times as the grid numbers were increased from 75×25 to 105×35. However, convergence of the magnitude of the oscillatory amplitude could not be obtained due to limitations in the available computational facilities. Surprisingly, the characteristic frequency of the oscillation was found to be independent of gridsize. Similar characteristics were obtained by Ozoe and Hara [30] for a horizontal layer (one depth to four lengths) of liquid metal heated from below. They studied the effect of the Prandtl number (0.1, 0.01, 0.001) and the gridsize. Both the magnitude and oscillatory amplitudes of the average Nusselt number were found with increasing grid meshes of 121×31, 161×41 and 201×51. Again convergence could not be obtained. However, the critical Rayleigh number for the occurrence of the oscillatory natural convection was found to be independent of gridsize. This value was found to be slightly greater than the critical Rayleigh number of 1708, which is similar to the experimental findings of Rossby [26].

This prior work on oscillatory natural convection of low-Prandtl-number fluids was all for two-dimensional systems. The present paper is concerned with a transient three-dimensional system.

2. Model and computational scheme

The computational region is shown in Fig. 1. The width and length are five times the height. The grid numbers are

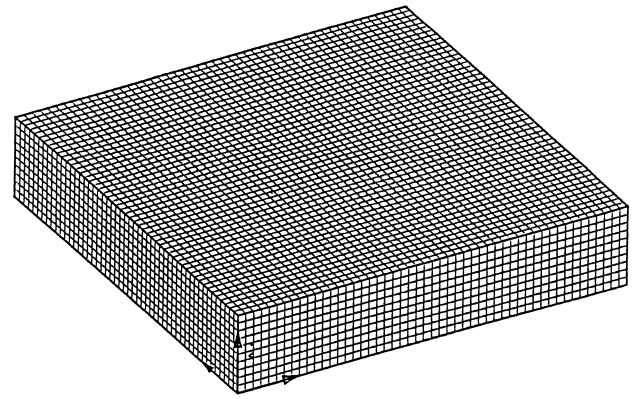

Fig. 1. Schematics of the computational regime with grids of $51 \times 51 \times 11$.

$51 \times 51 \times 11$. Fig. 2 shows top and side views of the coordinate system. By means of the dragless and adiabatic bounding vertical walls, this system simulates an infinitely wide shallow layer.

The equations are for transient conservation in an incompressible fluid except for the Boussinesq approximation in the buoyancy term. These equations may be written in non-dimensional form as follows:

$$\frac{\partial U}{\partial X} + \frac{\partial V}{\partial Y} + \frac{\partial W}{\partial Z} = 0 \tag{1}$$

$$\frac{\partial U}{\partial \tau} + \frac{U\partial U}{\partial X} + \frac{V\partial U}{\partial Y} + \frac{W\partial U}{\partial Z} = \frac{-\partial P}{\partial X} + \Pr\left(\frac{\partial^2 U}{\partial X^2} + \frac{\partial^2 U}{\partial Y^2} + \frac{\partial^2 U}{\partial Z^2}\right) \tag{2}$$

$$\frac{\partial V}{\partial \tau} + \frac{U\partial V}{\partial X} + \frac{V\partial V}{\partial Y} + \frac{W\partial V}{\partial Z} = \frac{-\partial P}{\partial Y} + \Pr\left(\frac{\partial^2 V}{\partial X^2} + \frac{\partial^2 V}{\partial Y^2} + \frac{\partial^2 V}{\partial Z^2}\right) \tag{3}$$

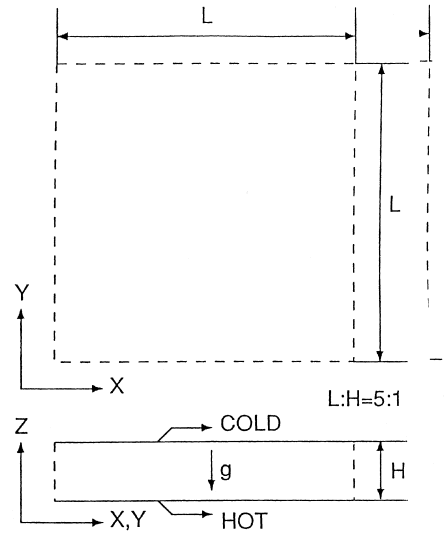

Fig. 2. Top and side views of the system.

$$\frac{\partial W}{\partial \tau}+\frac{U\partial W}{\partial X}+\frac{V\partial W}{\partial Y}+\frac{W\partial W}{\partial Z}=\frac{-\partial P}{\partial Z}+\mathrm{Pr}\left(\frac{\partial^2 W}{\partial X^2}+\frac{\partial^2 W}{\partial Y^2}+\frac{\partial^2 W}{\partial Z^2}\right)+\mathrm{Ra}\,\mathrm{Pr}(\theta+0.5-Z) \quad (4)$$

$$\frac{\partial \theta}{\partial \tau}+\frac{U\partial \theta}{\partial X}+\frac{V\partial \theta}{\partial Y}+\frac{W\partial \theta}{\partial Z}=\left(\frac{\partial^2 \theta}{\partial X^2}+\frac{\partial^2 \theta}{\partial Y^2}+\frac{\partial^2 \theta}{\partial Z^2}\right)+W \quad (5)$$

The dimensionless variables are defined as

$$X=\frac{x}{x_0},\qquad Y=\frac{y}{y_0},\qquad Z=\frac{z}{z_0},\qquad x_0=y_0=z_0=H$$

$$U=\frac{u}{u_0},\qquad V=\frac{v}{v_0},\qquad W=\frac{w}{w_0},\qquad u_0=v_0=w_0=\frac{\alpha}{x_0}=\frac{\alpha}{H}$$

$$\tau=\frac{t}{t_0},\quad t_0=\frac{x_0^2}{\alpha}=\frac{H^2}{\alpha}$$

$$P=\frac{p}{p_0},\quad p_0=\rho u_0^2=\frac{\rho\alpha^2}{H^2}$$

$$\Phi=\frac{T-T_0}{T_\mathrm{h}-T_\mathrm{c}},\qquad T_0=\frac{T_\mathrm{h}+T_\mathrm{c}}{2},\qquad \Phi_\mathrm{c}=0.5-Z,\quad \theta=\Phi-\Phi_\mathrm{c}=\Phi-0.5+Z$$

$$\mathrm{Pr}=\frac{\nu}{\alpha},\quad \mathrm{Ra}=\frac{g\beta(T_\mathrm{h}-T_\mathrm{c})H^3}{\alpha\nu}.$$

In these equations, θ represents temperature fluctuations about the conductive state Φ_c.

The boundary conditions are indicated in Fig. 3(a) and (b), for the $Y=$ constant and the $X=$ constant planes, respectively. As noted above, the four vertical side walls are dragless and have an adiabatic fluid interface. The bottom was kept at a higher temperature of +0.5 with the addition of absolute random variations of 10^{-5} or less in order to initiate convection. The temperature of the top plate was kept at −0.5.

The above equations of conservation were approximated by second-order central finite-differences, but with a first-order upwind scheme for the inertial terms when the grid Peclet number became larger than 2. The computational region was represented by staggered meshes and solved by the HSMAC (Highly Simplified Marker and Cell) method [31]. Computations were carried out with an IBM model 59H (132 M Flops). The present results were obtained from a 2-month-long run.

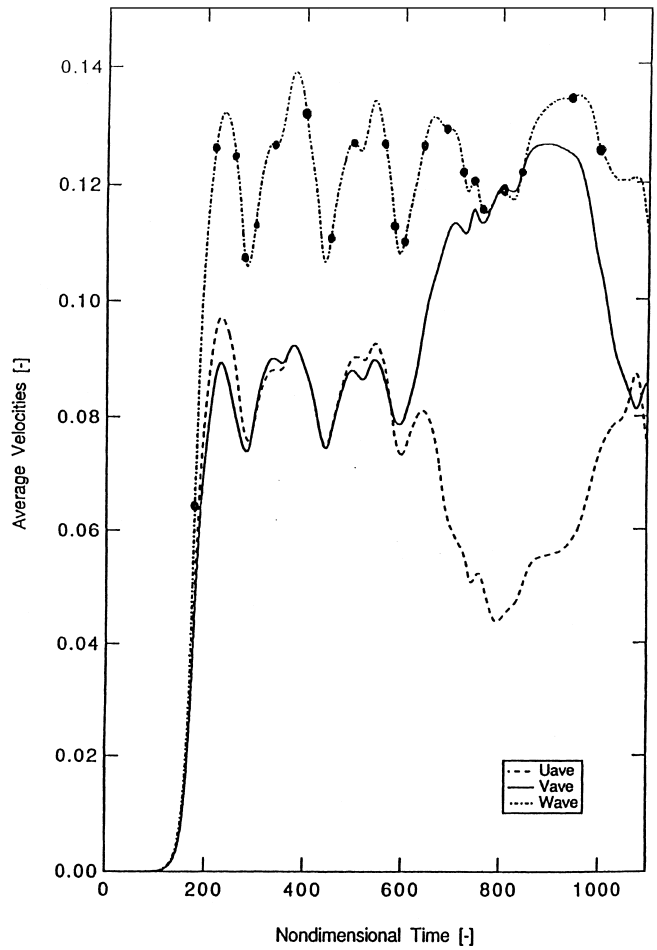

Fig. 4. Transient responses of the average velocity components in the *X*-, *Y*- and *Z*-directions for Pr = 0.01 and Ra = 2000.

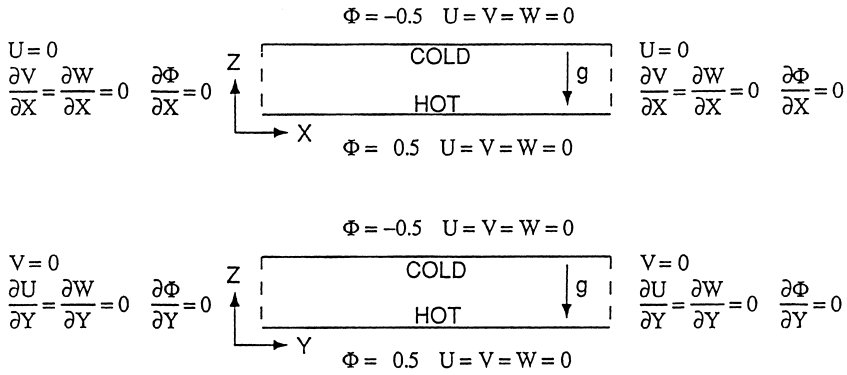

Fig. 3. Boundary conditions of the system. (a) For a *X*–*Z* (*Y* = constant) plane. (b) For a *Y*–*Z* (*X* = constant) plane.

3. Computed results

Computations were carried out for $Pr = 0.01$ and $Ra = 2000$. Fig. 4 shows the transient responses of the three components of velocity as averaged by summation of their squares in each cell, then division by the number of cells and square rooting. The two horizontal velocity components U and V are represented by the solid and hatched lines, respectively, and the vertical component W by the dotted line. The time step $\Delta\tau$ was 0.001. After about $\tau = 120$ (1.2×10^5 time steps), the velocity components all rose abruptly. This is somewhat similar to the physical instability caused by small external perturbations of the system. Then, at about $\tau = 200$, the velocity components started to oscillate. After three oscillations, the U and V components parted but again came back together at their original magnitude after about $\tau = 1000$. These peculiar transient characteristics may be understood by observing the velocity and temperature profiles at representative instances as follows.

Fig. 5 shows a series of instantaneous top views of horizontal velocity vectors in a square region of the $Z = 0.25$ plane. These 21 instances are indicated with black circles in Fig. 4 on the response curve for the W velocity component. In Fig. 5, at $\tau = 180$, about six to seven tetragonal or hexagonal cells were formed. These are typical of the Benard-type cells that result from quick heating. However, at $\tau = 220$, they became parallel roll cells with their axes in a horizontal and diagonal direction of the square region. After this, even more complicated modes of flow occurred, but at $\tau = 400$, 560 and 680, a similar diagonal roll-cell pattern appeared again. In these instances, the average W velocity component appears to have attained its peak value. At $\tau = 600$ or after, the U values decreased in magnitude, suggesting an orientation of roll cells in the

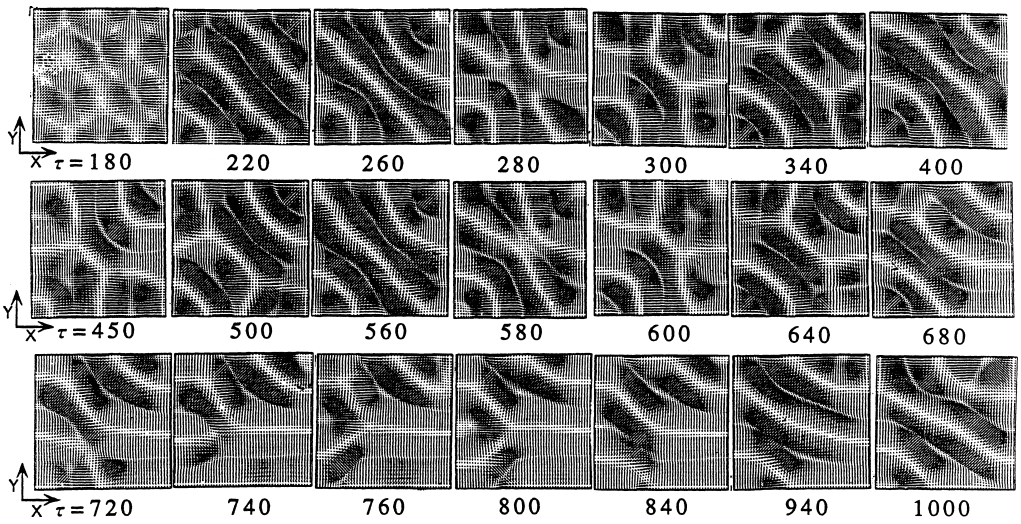

Fig. 5. A series of top views of instantaneous velocity vectors in the $Z = 0.25$ plane for $Pr = 0.01$ and $Ra = 2000$.

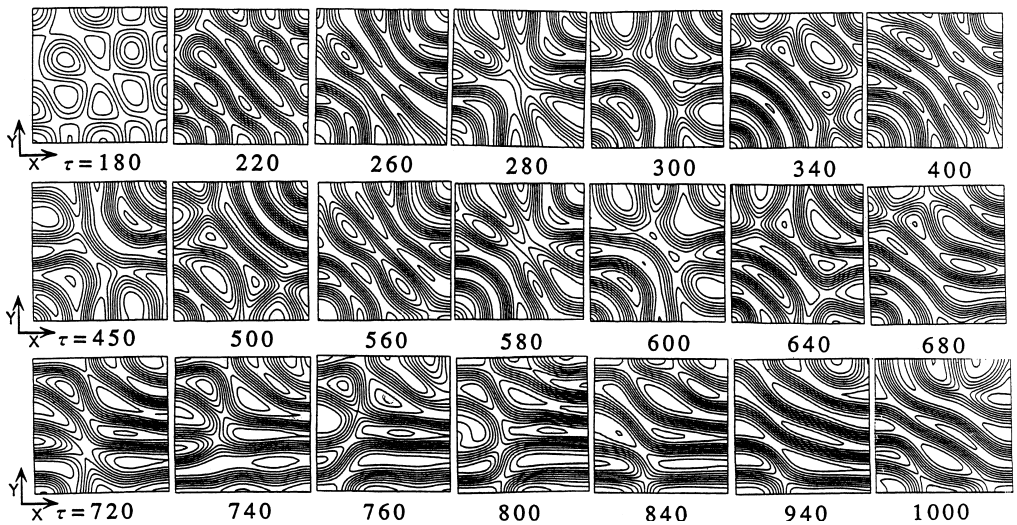

Fig. 6. A series of top views of instantaneous isotherms in the $Z = 0.25$ plane for $Pr = 0.01$ and $Ra = 2000$.

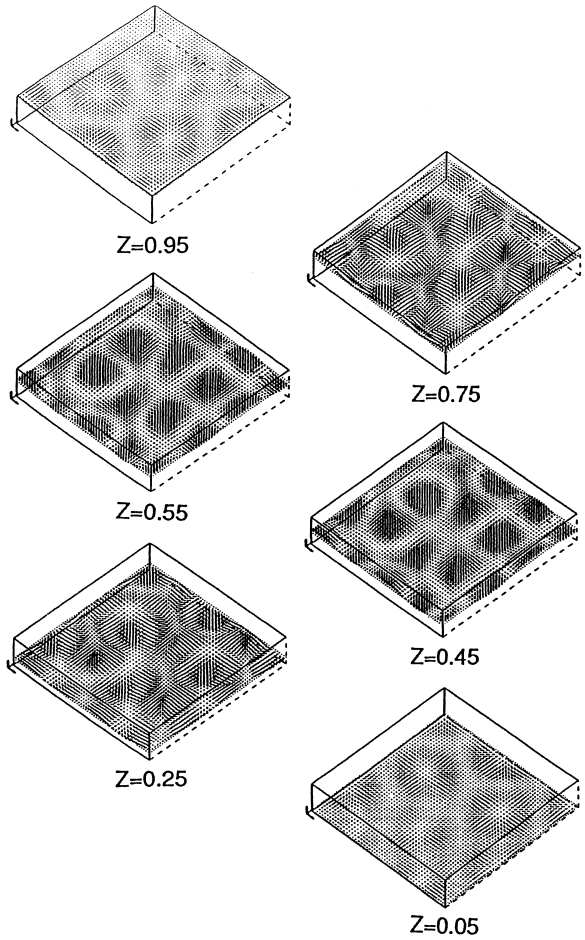

Fig. 7. Various perspective views of horizontal velocity vectors at various heights of $Z =$ constant at $\tau = 180$ for $\mathrm{Pr} = 0.01$ and $\mathrm{Ra} = 2000$.

X-direction. The graphs at $\tau = 720$ to 800 apparently represent dominant Y-velocity components and a strong increase in the V-velocity curves. At or after $\tau = 940$, the diagonal roll cells again appeared and attained a similar structure to that before. Because of the very long computing time (2 months), the computations were terminated at this point.

Fig. 6 shows corresponding instantaneous isotherms in the $Z = 0.25$ plane. At $\tau = 180$, multiple, separate, cylindrical cells appeared. However, at $\tau = 220$, parallel roll cells in the diagonal direction of the square region become dominant. The subsequent transient isotherms correspond to the velocity vectors shown in Fig. 5.

Fig. 7 shows velocity vectors at $\tau = 180$ at various depths of Z from 0.05 to 0.95. Similar horizontal velocity profiles for the tetragonal cells can be seen. Fig. 8(a) shows side-views at $\tau = 180$ and in the four different cross sections corresponding to $Y = 0.95$, 1.95, 2.95 and 3.95. Four rolls are apparent at $Y = 1.95$ and 2.95. Fig. 8(b) shows side-views at four different cross sections corresponding to $X = 0.95$, 1.95, 2.95 and 3.95. Three rolls can be seen at $X = 0.95$ and 3.95. These vertical cross sections correspond to the tetragonal cells.

Fig. 9 shows perspective views of the velocity vectors at $\tau = 800$, the time when the average velocity component U attains its minimum magnitude. The X-directional roll cells appear to be dominant at all heights. This is more apparent in the vertical cross sectional views as shown next.

Fig. 10 shows corresponding vertical side views in (a) the X–Z and (b) the Y–Z planes respectively. Fig. 10(a) shows vertical cross sections at various $Y =$ constant planes in which only one or two roll cells can be seen. On the other

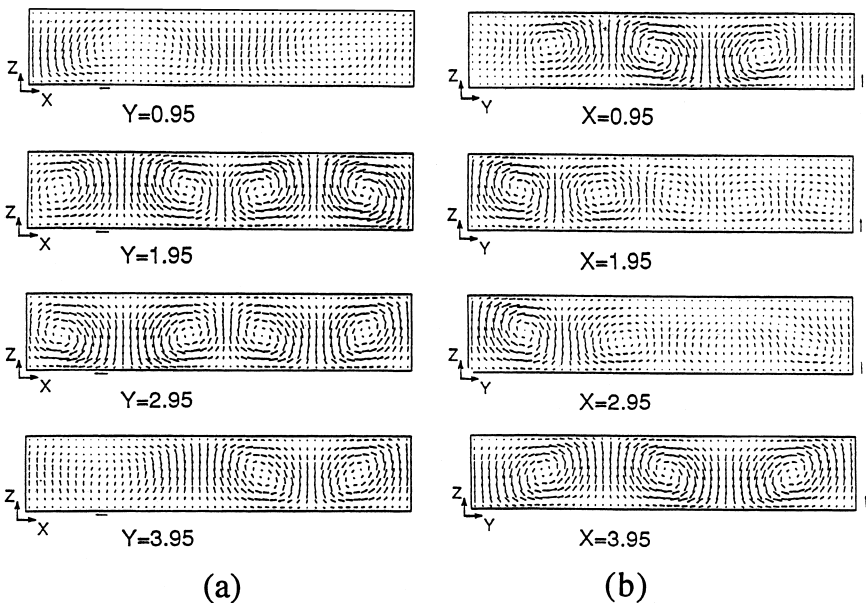

Fig. 8. (a) Velocity vectors in X–Z ($Y =$ constant) planes at $\tau = 180$ for $\mathrm{Pr} = 0.01$ and $\mathrm{Ra} = 2000$. (b) Velocity vectors in Y–Z ($X =$ constant) planes at $\tau = 180$ for $\mathrm{Pr} = 0.01$ and $\mathrm{Ra} = 2000$.

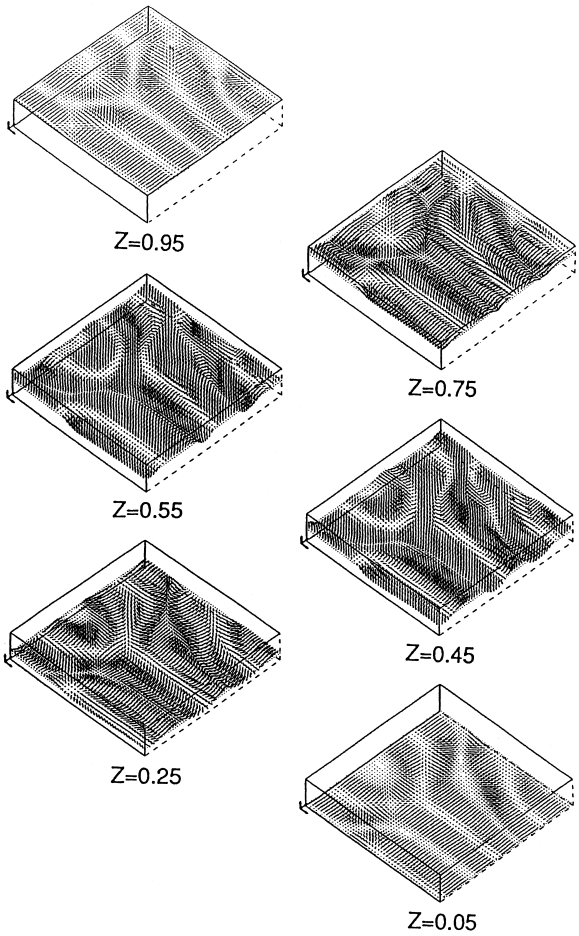

Fig. 9. Various perspective views of horizontal velocity profiles at various heights of Z = constant at $\tau = 800$ and for = 0.01 and Ra = 2000.

hand, Fig. 10(b) shows vertical cross sections at X = constant planes in which four to five much stronger roll cells are apparent. The large increase in the average V-velocity component as shown in Fig. 4 is a consequence of this orientation of the quasi two-dimensional roll cells.

Over this entire period of time, the average Nusselt number was about 1.001 or less, and hence is not plotted.

As mentioned in the introduction, convergence of the numerical computations for oscillatory natural convection in low-Prandtl-number fluids has not been attained with complete success even for two-dimensional systems. Some of the details of the present results for a three-dimensional system would also be expected to be dependent on gridsize. However, on the basis of the previous studies, the basic characteristics of the oscillations would be expected to be independent of gridsize. The computations are limited to a single aspect ratio, Pr = 0.01 and Ra = 2000. More extensive results may be expected with the present computational scheme as larger and faster computer facilities become available in the near future.

4. Conclusions

Transient three-dimensional numerical computations were successfully carried out for Benard-type roll-cells at Pr = 0.01 and Ra = 2000. The transient response after a step change in the wall temperature was at first a regular oscillation, which then evolved to a series of long roll-cells with their axes in one direction. The computations revealed coupling and decoupling of the roll cells. These predictions still need be tested with experimental measurements.

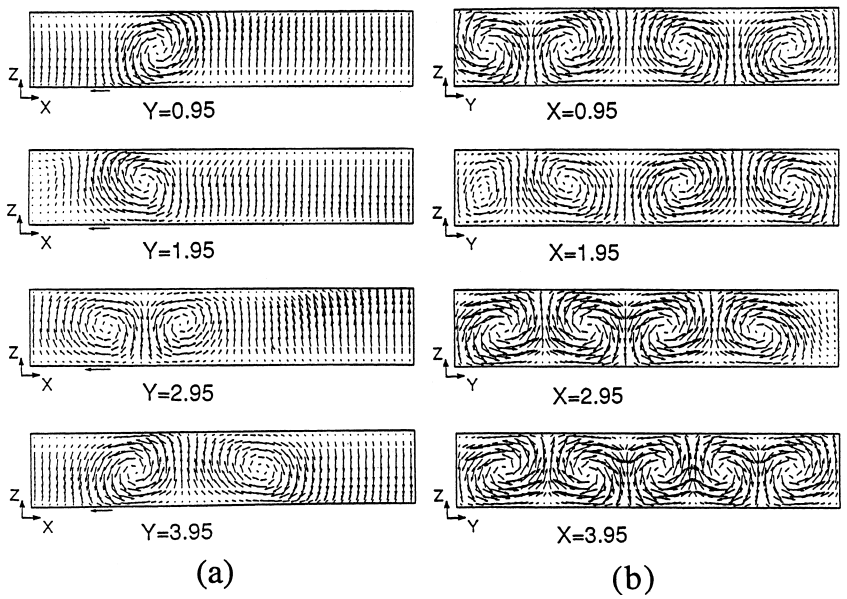

Fig. 10. (a) Velocity vectors in a vertical cross section at X–Z (Y = constant) planes at $\tau = 800$ for Pr = 0.01 and Ra = 2000. (b) Velocity vectors in a vertical cross section at Y–Z (X = constant) planes at $\tau = 800$ for Pr = 0.01 and Ra = 2000.

5. Nomenclature

Symbols

g	acceleration due to gravity (ms^{-2})
Gr	Grashof number $= g\beta(T_h - T_c)H^3/\nu^2$
H	height of a layer (m)
L	length of a layer (m)
Nu	average Nusselt number $qH/k(T_h - T_c)$
p	pressure (Pa)
P	$=p/p_0$
Pr	Prandtl number $= \nu/\alpha$
Ra	Rayleigh number $=$ GrPr
T	temperature (K)
T_c	cold wall temperature (K)
T_h	hot wall temperature (K)
T_0	average temperature $= (T_h + T_c)/2$
u	velocity component in the X direction (ms^{-1})
U	$=u/u_0$
v	velocity component in the Y direction (ms^{-1})
V	$=v/u_0$
w	velocity component in the Z direction (ms^{-1})
W	$=w/u_0$
x	horizontal coordinate (m)
X	$=x/H$
y	horizontal coordinate (m)
Y	$=y/H$
z	vertical coordinate (m)
Z	$=z/H$

Greek Symbls

α	thermal diffusivity ($m^2\ s^{-1}$)
β	volumetric coefficient of expansion (K^{-1})
Δ	difference
θ	$=\Phi$-$(Z-0.5)$
ν	kinematic viscosity ($m^2\ s^{-1}$)
τ	$=t\alpha/H^2$
Φ	dimensionless temperature $= (T-T_0)/(T_h-T_c)$

References

[1] D.T.J. Hurle, Temperature oscillation in molten metals and their relationship to growth striae in melt-grown crystals, Philos. Mag. 13 (1966) 305–310.

[2] A.E. Gill, A theory of thermal oscillations in liquid metals, J. Fluid Mech. 64 (1974) 577–588.

[3] M. Abricka, J. Krümins, Yu. Gelfgat, Numerical simulation of MHD rotator action on hydrodynamics and heat transfer in single crystal growth processes, J. Crystal Growth 180 (1997) 388–400.

[4] N. Ma, J.S. Walker, Validation of strong magnetic field asymptotic models for dopant transport during semiconductor crystal growth, J. Crystal Growth 180 (1997) 401–409.

[5] K. Kakimoto, M. Eguchi, H. Ozoe, Use of an inhomogeneous magnetic field for silicon crystal growth, J. Crystal Growth 180 (1997) 442–449.

[6] R. Assaker, N. Van den Bogaert, F. Dupret, Time-dependent simulation of the growth of large silicon crystals by the Chochralski technique using a turbulent model for melt convection, J. Crystal Growth 180 (1997) 450–460.

[7] E. Dornberger, E. Tomzig, A. Seidl, S. Schmitt, H.-J. Leister, Ch. Schmitt, G. Müller, Thermal simulation of the Czochralski silicon growth process by three different models and comparison with experimental results, J. Crystal Growth 180 (1997) 461–467.

[8] J. Järvinen, R. Nieminen, T. Tiihonen, Time-dependent simulation of Czochralski silicon crystal growth, J. Crystal Growth 180 (1997) 468–476.

[9] Y.-S. Lee, Ch.-H. Chun, Experiments on the oscillatory convection of low Prandtl number liquid in Czochralski configuration for crystal growth with cusp magnetic field, J. Crystal Growth 180 (1997) 477–486.

[10] M. Tanaka, M. Hasebe, N. Saito, Pattern transition of temperature distribution at Czochralski silicon melt surface, J. Crystal Growth 180 (1997) 487–496.

[11] J. Fainberg, H.-J. Leister, G. Müller, Numerical simulation of the LEC-growth of GaAs crystals with account of high-pressure gas convection, J. Crystal Growth 180 (1997) 517–523.

[12] K. Toh, H. Ozoe, Dopant concentration profile in a Czochralski flow of liquid metal in a vertical or a horizontal magnetic field, J. Crystal Growth 130 (1993) 645–656.

[13] M. Iwamoto, T. Hashimoto, K. Toh, H. Ozoe, Numerical computation of liquid encapsulated Czochralski bulk flow in comparison with flow visualization, J. Chem. Eng. Japan 27(3) (1994) 344–350.

[14] H. Ozoe, M. Iwamoto, Combined effects of crucible rotation and horizontal magnetic field on dopant concentration in a Czochralski melt, J. Crystal Growth 142 (1994) 236–244.

[15] H.J. Sung, Y.J. Jung, H. Ozoe, Prediction of transient oscillating flow in Czochralski convection, Int. J. Heat Mass Transfer 38(9) (1995) 1627–1636.

[16] Y. Shimabukuro, T. Tagawa, K. Kakimoto, H. Ozoe, Numerical computation for the Czochralski momentum, heat and mass transfer under a cusp-shaped magnetic field, The 3rd Int. Thermal Energy Congr., Kitakyushu, 1997, pp. 221–227.

[17] K. Kakimoto, H. Ozoe, Heat and mass transfer during crystal growth, Computational Mater. Sci. 10 (1998) 127–133.

[18] M. Akamatsu, K. Kakimoto, H. Ozoe, Numerical computation for the secondary convection in a Czochralski crystal growing system with a rotating crucible and a static crystal rod, J. Mater. Process. Manufacturing Sci. 5 (1998) 329–348.

[19] M. Akamatsu, K. Kakimoto, H. Ozoe. Numerical calculation of natural and mixed convection in a Czochralski crucible under transverse magnetic fields, Proc. 11th IHTC, Vol. 3, 1998, pp. 239–244.

[20] R. Krishnamurti, On the transition to turbulent convection, Parts 1 and 2, J. Fluid Mech. 42 (1970) 295–320.

[21] R.M. Clever, F.H. Busse, Transition to time-dependent convection, J. Fluid Mech. 65 (1974) 625–645.

[22] R.M. Clever, F.H. Busse, Low-Prandtl number convection in a layer heated from below, J. Fluid Mech. 102 (1981) 61–74.

[23] R.M. Clever, F.H. Busse, Convection at very low Prandtl numbers, Phys. Fluids, Ser. A 2(3) (1990) 339–344.

[24] G. Müller, G. Neumann, W. Weber, Natural convection in vertical Bridgman configurations, J. Crystal Growth 70 (1984) 78–93.

[25] J.R. Ristorcelli, J.L. Lumley, Instabilities, transition and turbulence in the Czochralski crystal melt, J. Crystal Growth 116 (1992) 447–460.

[26] H.T. Rossby, A study of Benard convection with and without rotation, J. Fluid Mech. 36(2) (1969) 309–335.

[27] K. Okada, H. Ozoe, The effect of aspect ratio on the critical Grashof number for oscillatory natural convection of zero Prandtl number fluid; numerical approach, J. Crystal Growth 126 (1993) 330–334.

[28] K. Okada, H. Ozoe, Various computational conditions of oscillatory natural convection of zero Prandtl number fluid in an open boat heated and cooled from opposing vertical walls, Numer. Heat Transfer 23 (1993) 171–187.
[29] T. Tagawa, H. Ozoe, Effect of Prandtl number and computational schemes on the oscillatory natural convection in an enclosure, Numer. Heat Transfer, Part A 30 (1996) 271–282.
[30] H. Ozoe, T. Hara, Numerical analysis for oscillatory natural convection of low Prandtl number fluid heated from below, Numer. Heat Transfer, Part A 27 (1995) 307–317.
[31] C.W. Hirt, B.D. Nichols, N.C. Romero, Technical Report Los Alamos Science Laboratory, 1975.